



Redox-responsive degradable microgel modified with superparamagnetic nanoparticles exhibiting controlled, hyperthermia-enhanced drug release

Serife Dagdelen¹, Marcin Mackiewicz¹, Magdalena Osial³, Ewelina Waleka-Bargiel^{1,2}, Jan Romanski⁴, Pawel Krynski⁴, and Marcin Karbarz^{1,*} 

¹ Faculty of Chemistry, Biological and Chemical Research Center, University of Warsaw, 101 Żwirki I Wigury Av, 02-089 Warsaw, PL, Poland

² Faculty of Chemistry, Warsaw University of Technology, Noakowskiego 3, 00-664 Warsaw, PL, Poland

³ Department of Theory of Continuous Media and Nanostructures, Institute of Fundamental Technological Research, Polish Academy of Sciences, Pawińskiego 5B, 05-106, Warsaw, PL, Poland

⁴ Faculty of Chemistry, University of Warsaw, Pasteura 1, 02-093, Warsaw, PL, Poland

Received: 24 August 2022

Accepted: 7 January 2023

© The Author(s) 2023

ABSTRACT

A novel degradable microgel based on poly(*N*-isopropylacrylamide) (pNIPA) cross-linked with *N,N'*-bisacryloylcystine (BISS) and containing superparamagnetic iron oxide nanoparticles (SPION@CA) was synthesized by semi-batch precipitation polymerization and examined as a potential hyperthermia-enhanced drug carrier. The pNIPA provided the microgel with temperature sensitivity, the BISS was responsible for degradation in the presence of glutathione (GSH) (an –S–S–bond reductor naturally present in cells), while the SPION@CA permitted remote control of temperature to improve drug release. The microgels exhibited volume phase transition temperature at ca. 34 °C, which is near the human body temperature, and were stable across a wide range of temperatures and ionic strengths, as well as in the blood plasma at 37 °C. It was found that the presence of SPION@CA in the polymer network of the microgels enabled the temperature to be increased up to 42 °C by an alternating magnetic field, and that increasing the temperature from 37 to 42 °C significantly enhanced the releasing of the anticancer drug doxorubicin (DOX). The highest DOX release (82%) was observed at pH 5, 42 °C, and in the presence of GSH, and the lowest (20%) at pH 7.4, 37 °C, and in the absence of GSH. MTT assay indicated that compared to free doxorubicin, the microgel particles loaded with doxorubicin have comparable cytotoxicity against MCF-7 cancer cells while being significantly less toxic to MCF-10A healthy cells.

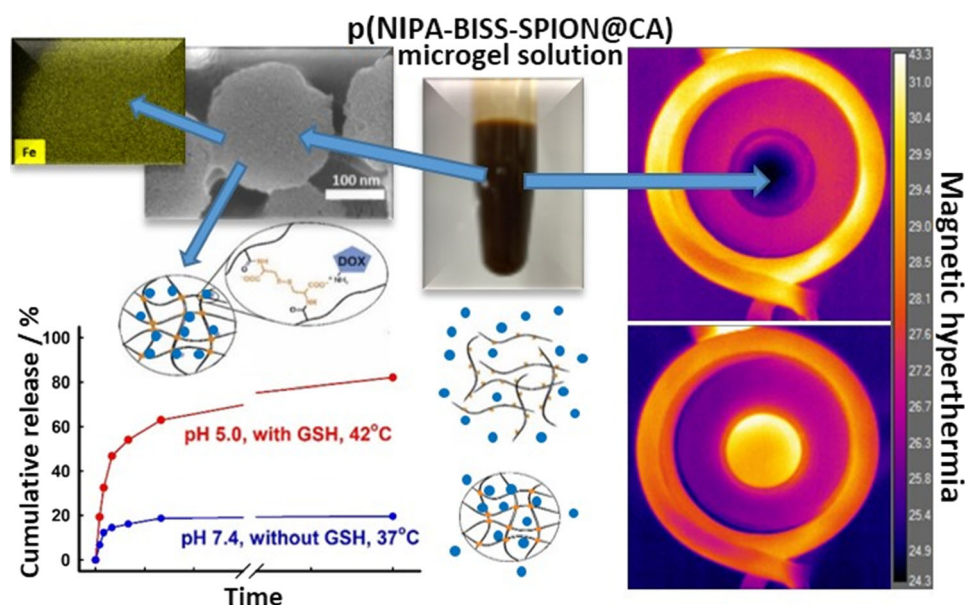
Handling Editor: Dale Huber.

Address correspondence to E-mail: karbarz@chem.uw.edu.pl

<https://doi.org/10.1007/s10853-023-08168-1>

Published online: 22 February 2023

GRAPHICAL ABSTRACT



Introduction

Cancer is one of the most fatal diseases in the world, for which a wide variety of treatments have been developed, including photodynamic therapy [1, 2], gene therapy [3], photothermal ablation [4], immunotherapy [5], radiation therapy [6] and chemotherapy combined with surgical treatment. Despite the recent advances in anticancer treatments, new solutions continue to be required, for instance, to address the various drawbacks of chemotherapy. The use of chemotherapeutic agents for cancer treatment involves many disadvantages, such as systemic toxicity, difficulties in targeting the drug to the tumor site, and low bioavailability of the drug [7]. The challenge of using chemotherapy to treat cancers lies in selectively eliminating tumor cells without affecting normal tissues. Various therapeutic approaches have been developed to increase the bioavailability of an antitumor drug and exert a significant impact on the desired target. Much research has been done in the field of nanomedicine [8], leading to the development of a series of nanocarrier materials, such as

micelles [9, 10], dendrimers [11, 12], hydrogels [13–17], and mesoporous silica [8, 18, 19]. Particularly promising among these are stimuli-responsive hydrogels: hydrogels that display a physicochemical response to external stimuli such as temperature or pH, which are being widely studied as potential drug carriers. This approach is motivated by tumor tissues' more acidic pH, higher levels of glutathione (GSH) in the cytoplasm, and higher temperature compared to normal tissues [20–23].

Hydrogels are chemically cross-linked polymers that are able to absorb large amounts of water, biological fluids, and toxic agents [24]. When the particle size of a hydrogel is below 100 nm, it is classified as a nanogel, and when it is between 100 and 100 μm , it is classified as a microgel [25, 26]. The most important advantages of microgels as drug carriers are their controlled particle size, simplicity of production, stability, and chemical topologies [21, 27–31]. Their 3D structure enables the encapsulation of hydrophobic or hydrophilic drugs within their internal network, potentially protecting these drugs from degradation during storage or from circulating in the blood. Microgels can change their volume,

wettability, and/or optical properties in response to environmental stimuli such as pH, temperature, electric or magnetic fields, light, solvent composition, solutes, and reduction/oxidation [32–40]. They can exist in two different states: swollen and collapsed (shrunken), and the transition from one state to another is called the volume phase transition [41]. Microgels based on poly(*N*-isopropylacrylamide) (pNIPA) are especially interesting in that they exhibit a volume phase transition temperature (VPTT) (~32 °C) that is close to the physiological temperature [41–44].

However, many temperature-sensitive polymers have a huge disadvantage: their non-degradability as a result of the presence of an indivisible crosslinker. Crosslinkers containing a disulfide bond (SS), diselenide bond (SeSe), or thioether bond (S), for instance, can be used to alleviate this. These redox-responsive linkers are frequently used in drug delivery systems [14, 35, 45–47]. The most common linker used in the synthesis of degradable microgels is *N,N'*-bisacryloylcystamine (BAC) [35, 45, 46, 48–51]. However, BAC is not soluble in water and does not give microgels stability in a solution of high ionic strength.

Herein we present a stimuli-sensitive microgel based on a cross-linking agent that we synthesized: *N,N'*-bisacryloylcystine (BISS) which, unlike BAC, contains carboxylic groups, is water-soluble and gives microgels pH sensitivity and stability in solutions of high ionic strength. Moreover, positively charged drugs can be bound to the ionized carboxylic groups of BISS through the use of electrostatic interactions. The cleavage of the disulfide bonds in such microgels by a reducing agent leads to the degradation of the microgels and releases the loaded drug. Thiols are well-known reducing agents, and one of them glutathione is present in most cancer cells at elevated concentrations [35]. Therefore microgels sensitive to this reducing agent can be expected to degrade and release a drug in cancer cells in a targeted manner.

There are many nanocomposite systems of hydrogels involving different types of nanoparticles, such as carbon nanotubes, clay, ceramic and metal nanoparticles, and magnetic nanoparticles [17, 52–57]. Superparamagnetic nanoparticles of iron oxide, with an average diameter of about 15 nm, are known to be very good candidates for biomedical applications [58]. They are widely used in nanocomposites for magnetic hyperthermia

application like magnetic aromatic polyamide [59], magnetic guanidinylated chitosan (MGC) nanobio-composite [60], iron oxide-hydroxyapatite nanocomposite [61], iron oxide @silver@ chitosan [62] and functionalized magnetic copper ferrite nanoparticles [63]. Recently, many research groups have focused on the use of SPIONs in cancer treatment by hyperthermia [64, 65].

Magnetic hydrogels have been investigated and applied in biomedical procedures, including magnetic separation for protein purification and separation of certain cell types, and are used as contrast agents in magnetic resonance imaging, in the treatment of tumors by hyperthermia techniques, and for the vectoring of drugs [66]. Such materials have particularly high potential as vectoring agents for the treatment of cancer, given their capacity for local delivery of chemotherapeutic agents in therapeutic doses, increasing treatment efficacy and decreasing adverse effects.

In this paper a novel degradable microgel based on poly(*N*-isopropylacrylamide) cross-linked with *N,N'*-bisacryloylcystine and containing superparamagnetic iron oxide nanoparticles is presented, as an anti-cancer drug carrier. The objective was to obtain a doxorubicin carrier that releases much more of the drug under conditions characteristic of cancer cells than under conditions characteristic of the blood circulatory system, with the ability to enhance such release through the magnetic hyperthermia effect.

Experimental

Chemicals

N-isopropylacrylamide (NIPA, 97%), ammonium persulfate (APS, 99.99%), L-glutathione reduced (GSH, 98%), and acryloyl chloride (96%) were purchased from Aldrich. Sodium hydroxide (NaOH, 99%), hydrochloric acid (HCl, 35–38%), *N,N,N',N'*-Tetramethyl ethylenediamine (TEMED), and L-cystine (98.5%) were purchased from POCH. Iron (III) chloride hexahydrate $\text{FeCl}_3 \cdot 6\text{H}_2\text{O}$ Aldrich ACS reagent 97%, and iron (II) chloride tetrahydrate $\text{FeCl}_2 \cdot 4\text{H}_2\text{O}$ p.a. ≥99% (RT), were supplied from Sigma-Aldrich (Sigma-Aldrich, St. Louis, MO, USA). 25% ammonia solution $\text{NH}_3(\text{aq})$ was supplied from POCH (Wroclaw, Poland). Citric acid was purchased from Sigma-Aldrich with a 94% grade. Acetone

having analytical grade was supplied from POCH. Doxorubicin hydrochloride (DOX) was purchased from LC Laboratories (Woburn, MA, USA).

All chemicals were used as provided by the manufacturers except for NIPA, which before experiments was recrystallized twice from the benzene/hexane mixture (9:1). All solutions were prepared using high-purity water obtained from a Hydrolab/HLP purification system (water conductivity: $0.056 \mu\text{S cm}^{-1}$).

N,N'-bisacryloylcystine cross-linker (BISS) were synthesized according to previously reported procedures [16]. Briefly, to obtain *N,N'*-bisacryloylcystine, into a stirred solution of sodium hydroxide and cystine in methanol, acryloyl chloride was added dropwise at 0°C . The solution was stirred at room temperature and after 4 h the reaction mixture was filtered through a celite pad. The filtrate was added dropwise into intensively stirred cold diethyl ether. The obtained suspended solid was isolated by filtration, washed with diethyl ether, and dried under a high vacuum at $30\text{--}45^\circ\text{C}$. The structure and purity of BISS were confirmed by ^1H MNR, ^{13}C MNR, mass spectroscopy, and by combustion analysis based on sulfur content.

Synthesis of superparamagnetic nanoparticles

Superparamagnetic iron oxide nanoparticles (SPION) were synthesized by the co-precipitation technique, where 540 mg of iron chloride hexahydrate $\text{FeCl}_3 \cdot 6\text{H}_2\text{O}$ and 200 mg of iron chloride tetrahydrate $\text{FeCl}_2 \cdot 4\text{H}_2\text{O}$ were dissolved in 10 mL of water and stirred magnetically with 1400 rpm, based on the procedure described by Gaweda et al. [67]. When salts were dissolved, the solution was heated on a hot plate to 80°C and ammonia aqueous solution was added until pH 10. The synthesis was performed in a glass vial. After the addition of ammonia into the solution, a dark precipitate formed, and the solution was continuously stirred for 10 min. After the synthesis, the glass vial was placed on a magnet to collect nanoparticles at the bottom of the vessel and the supernatant solution was poured off. Then, nanoparticles were washed several times with deionized water to remove unreacted compounds until neutral pH.

The following step involved the stabilization of nanoparticles with an organic coat to overcome the

aggregation of superparamagnetic iron oxide nanoparticles (SPION)s. The nanostructured precipitate was modified with citrates by the following procedure: 500 mg of citric acid was dissolved into 10 mL of deionized water, and then 0.5 M NaOH was added dropwise until pH 6 was reached. Then, the citrate solution was added to the glass vial with SPION (washed with Milli-Q water and collected on a magnet). Next, the solution was heated to 70°C and stirred at 500 rpm for 24 h to adsorb the citrates on the surface of nanoparticles. Then, the SPIONs modified with citrates (SPIONs@CA) were collected on the magnet, precipitated with acetone to separate excess citrates from the solution, and rinsed with water and acetone again. After washing, SPION@CAs were suspended in 20 mL of Milli-Q water and the suspension was ready for the following gel preparation.

Synthesis of NIPA-BISS/SPION@CA microgels

The microgel was synthesized using semi-batch precipitation polymerization (Fig. 1). Polymerization was conducted using a three-neck flask equipped with a reflux condenser, inlet, and outlet of inert gas. In the first step, the main monomer NIPA (0.187 g, 97 mM) and linker BISS (0.02 g, 3 mM) were dissolved in 15 mL of deionized water and placed in the flask. The mixture was heated to 70°C and deoxygenated for 0.5 h using argon. After mechanical stirring (250 rpm) for 1 h, an aqueous solution of APS (0.009 g in 2 mL deionized water) and 17 μL of TEMED were added to initiate the reaction. The pH of the solution was 5 and 1 mL of SPION@CA suspension was sonicated. Then, the SPION@CA were added drop-wise to the NIPA-BISS solution in the flask for 23 min with a peristaltic pump (2.6 mL h^{-1}). The reaction was allowed to proceed for 3 h, stopped by cooling the product to room temperature. The product was then dialyzed (dialysis tube with a 10,000 Da molecular weight cutoff-Spectra/Por® 7 Dialysis Membrane) against deionized water for one week to remove unreacted molecules. The dialysis water was changed two times every day. SPION@CA particles are large enough to be physically entrapped in the microgel polymer network during the polymerization process. However, physical interactions between SPION@CA particles and the polymer chains, e.g., like hydrogen bonds, are also possible.

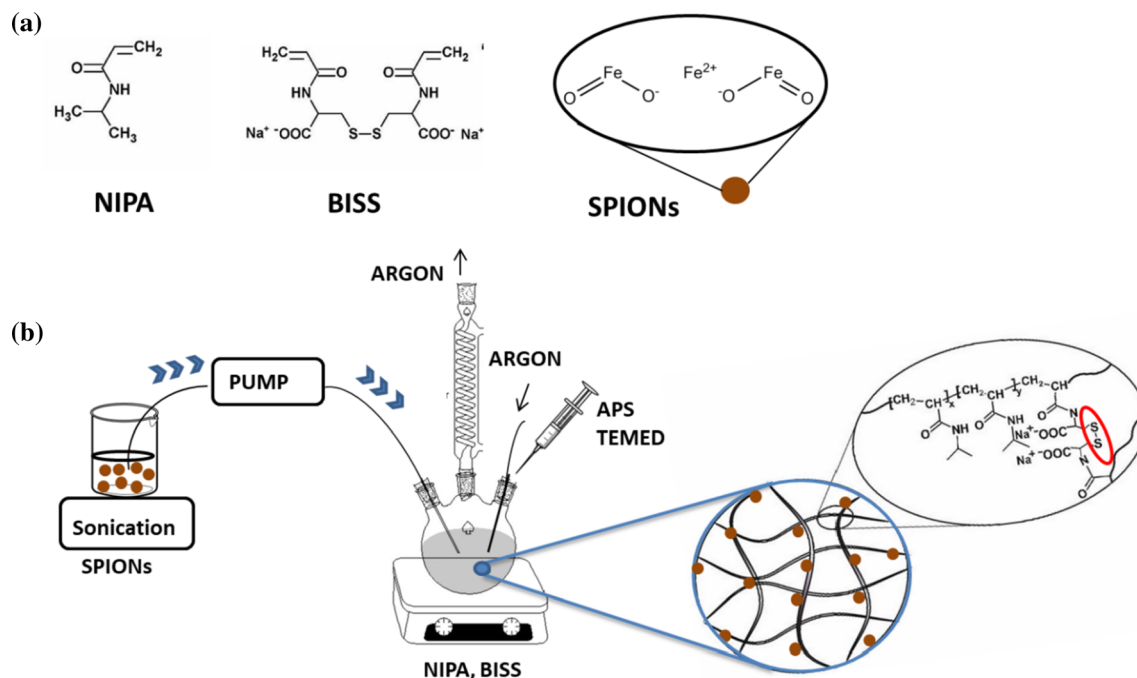


Figure 1 (a) Structure of chemicals used in microgel synthesis. (b) Scheme of synthesis of microgel based on *N*-isopropylacrylamide cross-linked with *N,N'*-bisacryloylcystine and modified with superparamagnetic iron nanoparticles (SPIONs) coated with citrates (CA).

Finally, the solution was centrifuged to separate untrapped SPION@CA particles. For comparison, the microgel without SPIONs was obtained under similar conditions.

Instrumental

Dynamic light scattering (DLS)

The hydrodynamic diameter of the particles was measured using a Malvern Zetasizer instrument (Nano ZS, UK) fitted with a 4 mW He–Ne laser ($\lambda = 632.8$ nm) as the light source at the scattering angle of 173° . The solutions were equilibrated at selected temperatures for 5 min before measurement. The ionic strength was kept constant at 0.01 M by adding NaCl.

Scanning electron microscopy (SEM)

The morphology and the elementary composition of microgels were investigated using a Merlin, ZEISS, Field Emission Scanning Electron Microscope (FE-SEM) coupled with a Quantax 400, Bruker, EDS/EDX detector. The samples were first dried completely at room temperature and next covered with a

thin layer of sputtered Au–Pd alloy to a depth of approximately 3 nm using a Polaron SC7620 Mini Sputter Coater.

Transmission electron microscopy (TEM)

The size and size distribution of SPION@CA were assessed with Transmission Electron Microscopy (TEM)-EF-TEM, Zeiss Libra 120 Plus, Stuttgart, Germany, operating at 120 kV.

Vibrating sample magnetometer

The magnetic properties were measured using vibrating sample magnetometer (VSM) at 309 K under the maximum applied field 10 kOe.

Thermogravimetric analysis

The citrate content on the SPION@CA was determined using thermogravimetric analysis (TGA Q50 (TA Instruments)), New Castle, PA, USA, under the ambient atmosphere in the temperature range from room temperature to 600°C , with a heating rate of $10^\circ\text{C min}^{-1}$.

Magnetic hyperthermia (MH)

The magnetic hyperthermia (MH) measurements were performed with nanoScale Biomagnetics D5 Series equipment with CAL1 CoilSet. The SAR values were estimated using MaNIaC Controller software (nB nanoScale Biomagnetics, Zaragoza, Spain). The microgel's temperature increase was also investigated with FLIR thermal imaging camera coupled with ResearchIR software.

Sample preparation for examination of the influence of temperature, pH, ionic strength, and reducing agents on properties of p(NIPA-BISS-SPION@CA) microgels

Dialysis-purified p(NIPA-BISS-SPION@CA) microgels were mixed with aqueous solutions of different pH and ionic strength and the presence of the reducing agent (GSH). pH was changed by adding either HCl or NaOH and was monitored with a pH/ion meter (Mettler Toledo, model SevenGo-SG2). The final pH value was measured just before the measurements. The ionic strength was kept at a constant level (0.01 M) by adding NaCl. Additionally, in all experiments where reducing agents were used, pH was kept close to 5.0.

Mathematical modeling of in vitro drug-release kinetics

The Higuchi, first-order, Weibull, Gompertz, and Korsmeyer–Peppas models were used to evaluate the kinetics of the DOX-release process. The equations of these models are presented in Table 1. The Higuchi model of release kinetics describes drug release as a square-root time-dependent diffusion process, in other words as Fickian diffusion of the drug from an insoluble matrix [42, 68–70]. The simplified first-order model shows that the release rate depends on the concentration, which was obtained from the plot of the log of the remaining drug versus time. The Weibull model describes the procedures related to a limited time based on distribution theory; this model is more useful for comparing the release profiles in matrix-type drug delivery [71]. The Gompertz model has a steep increase at the beginning and slowly converges to the asymptotic maximal dissolution [33, 72]; this model is more suitable for drugs with good solubility and intermediate release rate. The Korsmeyer–Peppas model expands on the simplified Higuchi model and proposes a power law where the drug-release fraction is proportional to time to the power of n , the release exponent [73]; this kinetic model is used for drug release from polymeric systems [74].

Table 1 Mathematical models of drug-release kinetics

Model	Equation	Variables and parameters
Higuchi	$Q_t = k_H t^{1/2}$	Q_t = amount of drug released in time t k_H = Higuchi dissolution constant
First-order	$\log Q_t = \log Q_0 - kt/2.303$	Q_t = fraction of drug released in time t Q_0 = initial concentration of drug k = first-order rate constant
Weibull	$Q_t = Q_0(1 - e^{-k(t-T)})$	Q_0 = the initial amount of the drug t = the time scale T = the total release time k = the rate constant of the Weibull
Gompertz	$Q_t = Q_{\max} \exp[-\alpha e^{\beta \log t}]$	$Q(t)$ = percent dissolved at time t divided by one hundred; Q_{\max} = maximum dissolution; α undissolved proportion at time $t=1$ β = dissolution rate per unit of time
Korsmeyer–Peppas	$Q_t = k_{KP} t^n$	Q_t = fraction of drug released in time t k_{KP} = release constant incorporating the structural and geometric characteristics of a drug-polymer system n = release exponent indicating the drug-release mechanism

The Korsmeyer–Peppas model superposes diffusion and swelling as independent mechanisms of release. The value n indicates whether drug release is governed by diffusion (Fickian model, case I) if $n=0.5$, or by swelling (non-Fickian model, case II) if $n=1.0$. These values of n are based on the geometry of the nanocarrier and are lower for spherical polymeric nanocarriers such as micro-nanogels (Table 3). The Korsmeyer–Peppas model depicts the release behavior well only up to a fractional release of 60% and cannot be utilized to describe near-maximum drug release in many cases.

Cell examination

MCF-10A (normal human mammary epithelial cells) and MCF-7 (human breast cancer cells), were purchased from American Type Culture Collection (ATCC). Cell viability was determined using MTT (3-(4,5-dimethylthiazol-2-yl)-2,5-diphenyltetrazolium bromide) colorimetric assay. After 24 h, the medium containing DOX, the p (NIPA-BISS-SPION@CA) microgel, and the p (NIPA-BISS-SPION@CA) microgel containing DOX was added to the cells and incubated for 72 h. 50 μL /well of MTT solution was added to each well. Formed formazan crystals were dissolved in 200 μL of 2-propanol. Absorbance was then measured at 570 nm with an ELX800 Absorbance Microplate Reader (BioTek Instruments). The IC₅₀ values for DOX and microgel containing DOX were determined using GraphPad Prism 7 (GraphPad Software) and the nonlinear regression analysis of the best fit Hill slope curve. The values are expressed as the mean value \pm standard deviation (S.D.) from two independent experiments ($n=6$). The effectiveness of penetration of the cells by the drug carriers was determined using a confocal microscope (Fluoview Olympus FV10i). All examined cells were cultured at 37 °C in an atmosphere enriched with 5% CO₂. Dulbecco's Modified Eagle Medium (DMEM, BioWest) containing 1% mixture of penicillin and streptomycin (BioWest), 10% fetal bovine serum (FBS, Gibco), and 1% of L-glutamine (BioWest) was used to cultivate MCF-7. MCF-10A was grown in DMEM supplemented with 5% horse serum, 10 ng mL⁻¹ epithelial growth factor, 5 μg mL⁻¹ hydrocortisone, and 10 μg mL⁻¹ human insulin.

Determination of DOX load and release

Loading of DOX

DOX, as a model anticancer drug, was selected to investigate the efficiency of drug loading and

consecutive controlled release into and from the p (NIPA-BISS-SPION@CA) microgels, respectively. DOX loading into the microgels was carried out via the incubation method. A portion of p (NIPA-BISS-SPION@CA) microgels (13 mg) was mixed with 4 mL of phosphate buffer solution (pH 7.4; 0.1 M). Next, 2 mg of DOX was added. The mixed solution was kept for 1 h at 37 °C, and next was kept overnight at 25 °C without stirring to allow DOX to reach the sorption equilibrium in the microgels. The obtained gel dispersion was purified by dialysis in water to collect the DOX-loaded p (NIPA-BISS-SPION@CA) microgels and to remove the unabsorbed DOX. The DOX amount loaded in p (NIPA-BISS-SPION@CA) microgels was calculated by subtracting the weight of DOX in the dialysate from the initial mass of DOX. The concentration/mass of DOX was determined spectrophotometrically by measuring absorbance at 480 nm and using the calibration curve.

In vitro drug release

The efficiency of the release of the drug from p (NIPA-BISS-SPION@CA) microgels was evaluated by employing the dialysis approach. The DOX-loaded p (NIPA-BISS-SPION@CA) microgels containing a known amount of DOX were dispersed in 1 mL of either a phosphate buffer of pH 7.4 or acetate buffer (pH 5.0) and transferred into a dialysis bag (MWCO, 10 kDa). The bags were dialyzed against 9 mL of the corresponding buffer (pH 7.4 or 5.0) containing 40 mM GSH or without GSH and gently stirred (100 rpm) at 37 °C or 42 °C. The released drug was sampled outside the dialysis bag and the concentration of released DOX was determined by measuring the absorbance at 480 nm.

Results and discussion

Characterization of SPION@CA and p (NIPA-BISS-SPION@CA) microgel

Firstly, the morphology of the obtained SPION@CA was investigated with transmission electron microscopy (TEM). Figure 2a reveals the spherical structures sized about 15 nm on average, see histogram. As can be seen, the nanoparticles have a quite uniform shape and size. Complementary to the TEM images, scanning electron microscopy (SEM) was

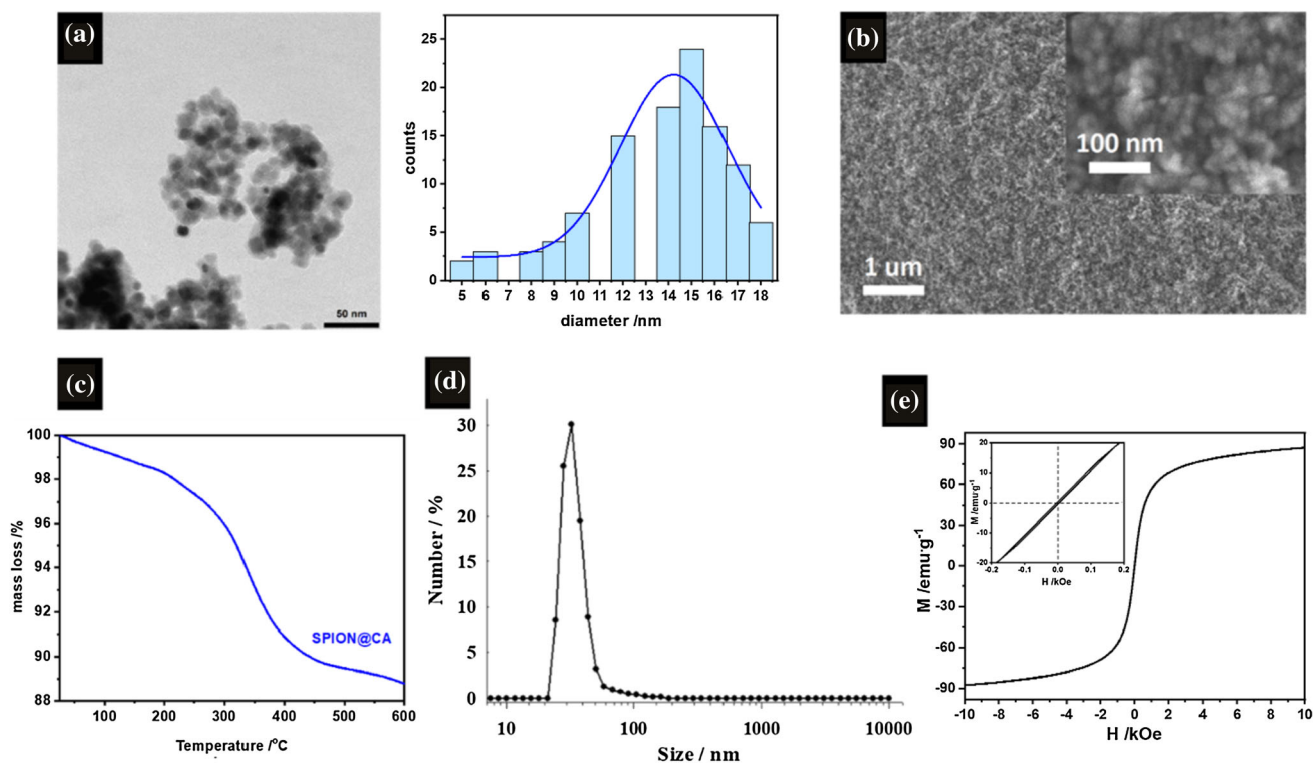


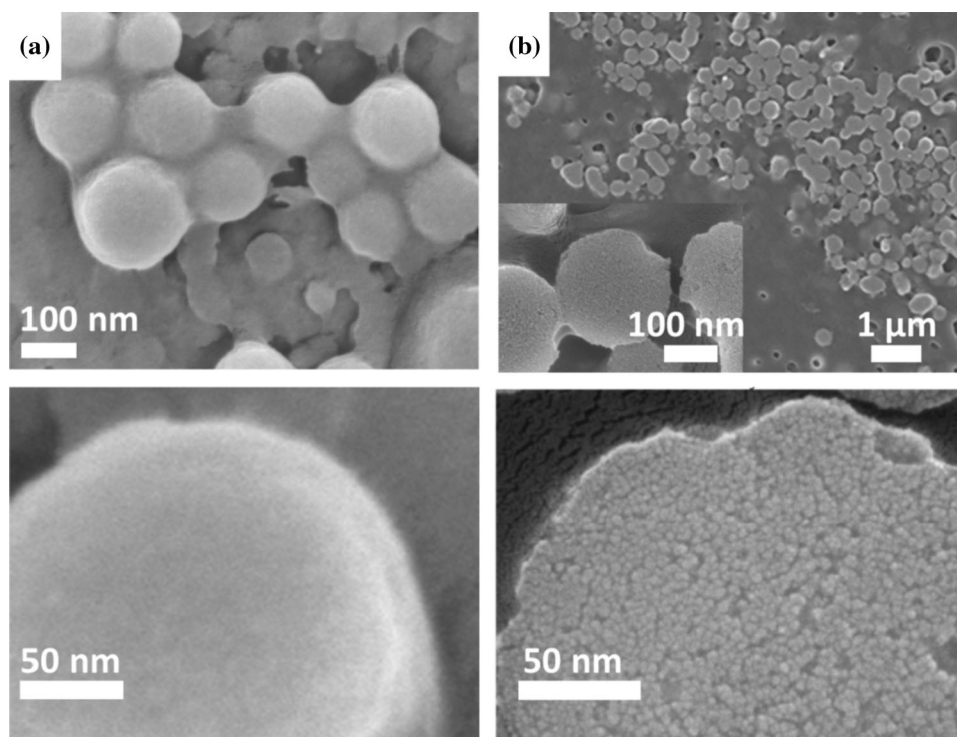
Figure 2 TEM images and the histogram of nanoparticles' size distribution (a), SEM image (b), thermogravimetric analysis of SPION@CA (c), distribution of size (hydrodynamic diameter) of SPION@CA in aqueous solution (d), and magnetization curve of bare SPION (e).

used to investigate the morphology of SPION@CA. As Fig. 2b shows, the nanoparticles within the whole bulk have a uniform shape and size. Next, the citrate content in the SPION@CA was determined using of thermogravimetry (TGA). Figure 2c presents the gradual mass loss for SPION@CA of ca. 2% caused by the water desorption from the surface (up to ca. 200 °C), followed by ca. 10% mass loss for SPION@CA caused by the decomposition of the citrates confirming successful coating of the pristine SPIONs core with citrates. Then, the hydrodynamic diameter of the SPION@CA particles was determined by DLS methods. To this end, an aqueous solution of SPION@CA was prepared, and just prior to the measurement the solution was sonicated. The size distribution of SPION@CA is presented in Fig. 2d. The size measured by DLS (~ 45 nm of hydrodynamic diameter) is significantly larger than the size of particles in the dried state measured by the electron microscope. This can be explained by the large solvation sphere surrounding SPION@CA in the solution, absent under the vacuum conditions of TEM

measurements. The presence of such a sphere significantly increases the dynamic diameter of citrate-coated nanoparticles. As the proposed material is planned to be used in the magnetic hyperthermia, the magnetic properties were studied with magnetometry. Figure 2e presents the narrow hysteresis loop (seen at inset). The magnetization saturation M_s in 309 K is ca. 86 emu g⁻¹.

Then, a p (NIPA-BISS-SPION@CA) microgel based on N -isopropylacrylamide (NIPA), degradable crosslinker N,N' -bisacryloylcystine (BISS), and contained SPION@CA was synthesized. The microgels were synthesized using semi-batch precipitation polymerization and to minimize/avoid the SPIONs aggregation, SPION@CA solution was introduced into the reactor using a pump and subjected to continuous sonication. For comparison, a microgel without SPION@CA (p (NIPA-BISS)) was also obtained. After the purification process the morphologies of the p (NIPA-BISS-SPION@CA) and p (NIPA-BISS) were investigated using SEM and results are presented in Fig. 3. As Fig. 3a shows, the p (NIPA-BISS) microgel

Figure 3 SEM images of the *p*(NIPA-BISS) microgels (column a) and *p*(NIPA-BISS-SPION@CA) microgels (column b).



forms rather smooth and spherical particles with the size of ca. 180 nm. The *p*(NIPA-BISS-SPION@CA) microgel also created rather spherical particles with a size of ca. 200 nm; however, the surface of the particles is non-uniform and graininess is clearly visible. This can suggest a porous structure with developed surface an asset from the point of view of the adsorptive drug load.

Next, further analysis of the *p*(NIPA-BISS-SPION@CA) microgel was performed using the EDS/EDX elemental mapping method. For the selected area of the microgel particles (Fig. 4a) the compositional mappings of iron, oxygen and nitrogen were done (Fig. 4b–d). The yellow spots, attesting to the presence of iron from SPION@CA particles, are observed only in the microgel area and are uniformly distributed, which confirms that the magnetic particles were successfully incorporated into the microgel. In addition, a similar distribution of oxygen, from SPION@CA and the polymer network, and nitrogen from the polymer network is well visible.

The stability a very important parameter of the SPION@CA, *p*(NIPA-BISS) microgel, and *p*(NIPA-BISS-SPION@CA) microgel was then investigated. To this end, three solutions were prepared and sonicated for 30 min. and observed for 1 week. The photos of the solutions are presented in Fig. 5. The solution of

SPION@CA was not stable and even after 1 day the sedimentation process is readily apparent (Fig. 5a), and after 1 week almost all SPION@CA particles aggregated and underwent sedimentation. For the *p*(NIPA-BISS) microgel solution, no visible changes were observed even after one week (Fig. 5b). Moreover, it was found that the suspension of *p*(NIPA-BISS-SPION@CA) microgels was stable (lack of visual sedimentation) for at least one week.

Then, the hydrodynamic diameter of the *p*(NIPA-BISS-SPION@CA) microgel in an aqueous solution was investigated as a function of temperature using the DLS technique. The obtained results are presented in Fig. 6a. As is visible, the microgel underwent the volume phase transition (VPT) from the swollen to the shrunken state at ca. 34 °C, a behavior that is typical for hydrogels based on poly(*N*-isopropylacrylamide) [75]. In addition, the VPT temperature measured for the *p*(NIPA-BISS) microgel was also ca. 34 °C. It suggests/confirms that SPION@CA particles do not significantly interact with polymer chains and are only physically trapped in the polymer network. The *p*(NIPA-BISS-SPION@CA) microgel particles shrank when the temperature exceeded the VPT temperature, and their diameter decreased from ca. 350 to 210 nm. The stability of *p*(NIPA-BISS-SPION@CA) microgel at

Figure 4 SEM image (a) and EDS/EDX elemental mapping of iron (b), oxygen (c), and nitrogen (d) in the $p(\text{NIPA-BISS-SPION@CA})$ microparticles.

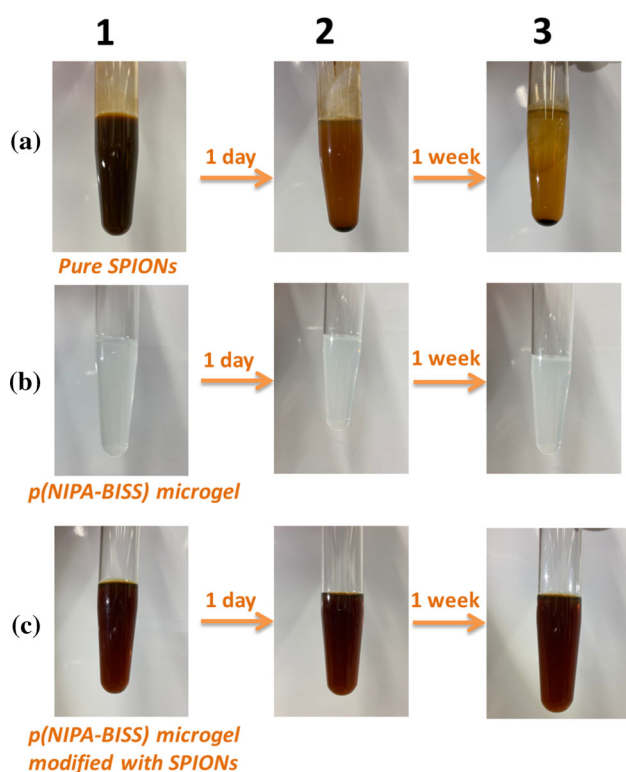
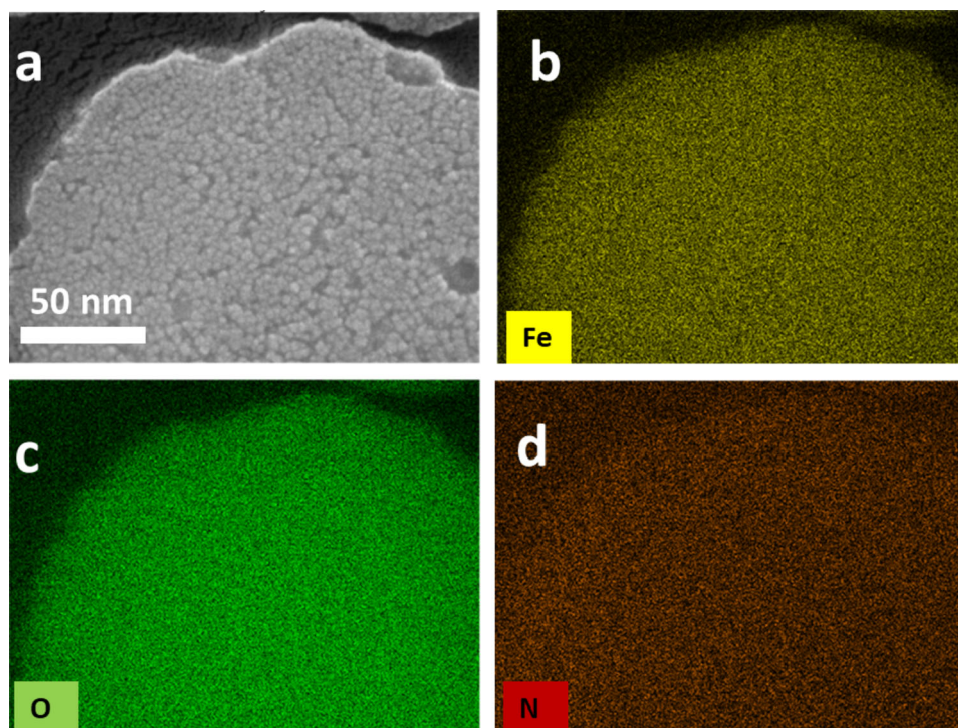
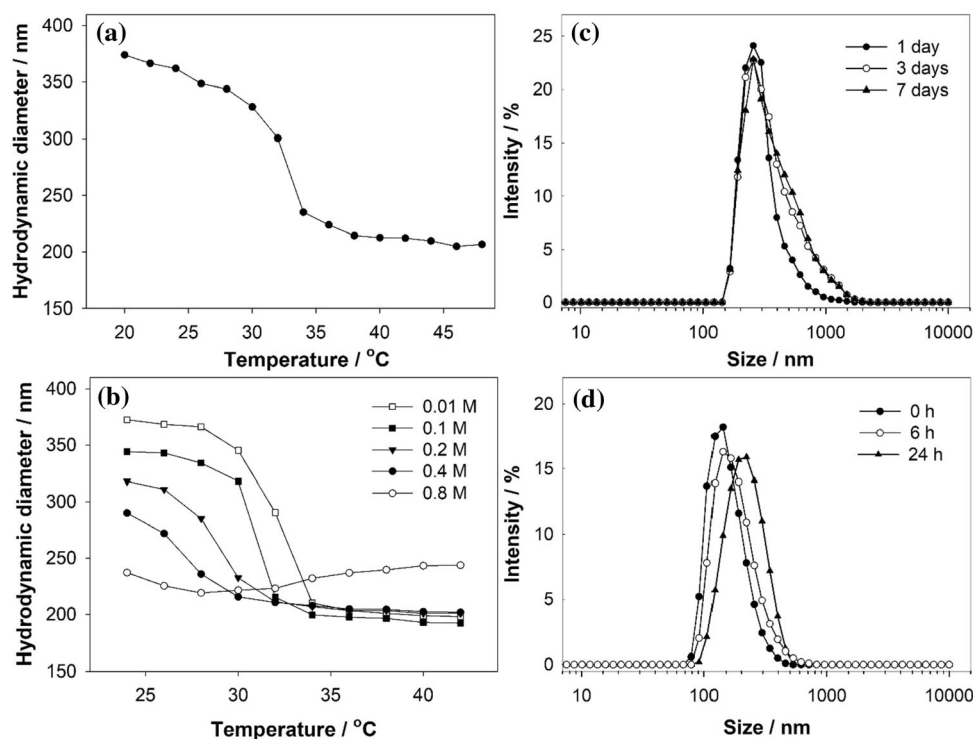


Figure 5 Photos of an aqueous solution of SPION@CA (a), $p(\text{NIPA-BISS})$ microgel (b), and $p(\text{NIPA-BISS-SPION@CA})$ microgel (c) immediately after sonication, after 1 day, and 1-week storage at room temperature.

various ionic strengths was also investigated as a function of temperature (Fig. 6b). Excellent stability vs. salt concentration was exhibited by the microgel. Up to 0.8 M concentration of NaCl, no aggregation was observed. As Fig. 6b shows, an increase in salt concentration caused a decrease in the volume of the gel before VPT and the temperature of this phenomenon also decreased. At 0.8 M NaCl, the microgel solution lost its typical temperature sensitivity and microgels were shrunken in the entire temperature range. It was found that at 1 M NaCl the microgels aggregated even at room temperature. The decrease in diameter value with the addition of salt is due to the Debye screening effect [76, 77]. When the Debye screening is sufficiently high microgels start to be unstable and aggregated when the temperature went up, especially when the temperature increased above the cloud-point/volume-phase-transition temperature. Generally, microgels based on *N*-isopropylacrylamide flocculated in the shrunken state when the electrolyte concentration is sufficiently high and the electrostatic repulsions between them are weakened [75]. The $p(\text{NIPA-BISS-SPION@CA})$ microgel is resistant to the flocculation process in a wide range of ionic strengths because it contains ionized groups and is strongly charged. Importantly, the microgel solution was stable under conditions similar to

Figure 6 Hydrodynamic diameter of *p*(NIPA-BISS-SPION@CA) microgel plotted vs. temperature in aqueous solution without addition a salt (a) and in solutions of different salt (NaCl) concentrations (b) size distribution of the microgel in water at 25 °C (c) and size distribution of the microgel in blood plasma at 37 °C (d).



physiological ones, e.g., 37 °C and 0.15 M of ionic strength. Finally, the stability of the *p*(NIPA-BISS-SPION@CA) microgel in water (25 °C) and blood plasma (37 °C) was investigated. Plots of size distribution after 1 day, 3 days and 7 days (in water), and 1 h, 6 h and 24 h (in blood plasma), are presented in Fig. 6C and Fig. 6D, respectively. As it can see in the both cases the solutions are quite stable over the time periods studied. In addition, zeta potential for was also measure and the value was -12.7 mV, -11.6 mV and -12.1 mV after 1 day, 3 day and 7 days, respectively. In addition, zeta potentials in the aqueous solution were measured and obtained values were: -12.7 mV, -11.6 mV and -12.1 mV after 1 day, 3 day and 7 days, respectively.

Next, the thermo-sensitivity of the microgels was investigated after their interactions with GSH (a disulfide reductor naturally present in cells). The corresponding changes in hydrodynamic diameter were plotted as functions of temperature for microgels and are presented in Fig. 7a. The degradation process was found to consist of three successive steps. In the first step (1 h), a decrease in the swelling degree of the microgel before and after VPT was seen: the reduction of the cross-linker simply caused a partial disintegration of the polymer network and a reduction in the volume of the microgel. In the second step (3 h), a

significant decrease in the size of the microgel before VPT was seen. Moreover, the observed temperature behavior is rather typical for pNIPA polymers. These polymers are soluble in water below VPT temperature, and precipitated and aggregate above VPT temperature (an increase in size) [22, 75]. Finally, after 24 h, in the whole temperature range, the size of measured particles is ca. 50 nm which is characteristic of SPION@CA. Distributions of hydrodynamic diameter of microgels untreated with GSH and treated with GSH after 3 h and 24 h at 25 °C are presented in Fig. 7b. The number average-size distributions approach was selected in this study, since it offered the smallest errors in the determination of the size distribution [78]. As can be seen, the size of microgels decreased from ca. 330 nm to 45 nm, due to the disintegration of microgel into polymers and iron nanoparticles (SPION@CA).

It is also known that reduction-resistant thioethers can be formed during precipitation polymerization of monomers containing the disulfide bond carried out at high temperatures [79]. Breaking of the disulfide bonds at high temperatures may lead to the formation of sulfur radicals that can form thioethers. However, the potentially formed thioethers have no significant effect on the degradation of the *p*(NIPA-BISS-SPION@CA) microgel under reducing conditions. In addition, the inflamed tissue, including

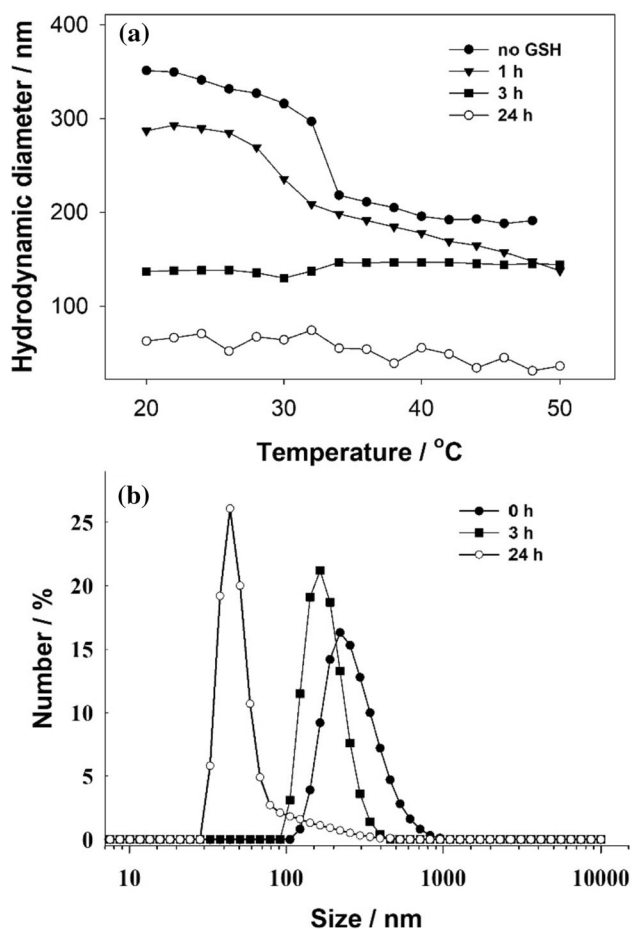


Figure 7 Hydrodynamic diameter plotted vs. temperature for microgels after different times of treatment with 40 mM GSH (a). Distribution of size of microgel particles before and after their degradation by GSH at 25 °C (b).

some cancer tissues, exhibit increased levels of reactive oxygen species (ROS), especially hydrogen peroxide. It was presented that microgel capsules based on poly(*N*-isopropylacrylamide) (NIPA) cross-linked with diacryloyl derivative of cysteine (BISS) can be degraded in the presence of hydrogen peroxide [80]. However, degradation of microgel capsules occurred at hydrogen peroxide concentrations much higher than physiological. Thus, it can be concluded that the *p*(NIPA-BISS-SPION@CA) microgel administered intravenously can only be degraded in a cell-reducing environment.

Magnetic hyperthermia investigations

The magnetic hyperthermia (MH) was used to study the heating efficiency *p*(NIPA-BISS-SPION@CA) microgel under the application of the alternating

magnetic field (AMF). The energy conversion into heat by SPION@CA takes place due to the relaxation of the superparamagnetic core due to the Néel and Brown modes. The microgel with a volume of about 0.5 mL containing magnetic particles of about 9 mg mL⁻¹ was placed in the copper coil, where it was thermostated at room temperature. The measurements were performed with alternating magnetic fields in the frequency range 386–633 kHz and with an amplitude of up to 30 kA m⁻¹, similarly to the conditions used in the literature for magnetic cross-linked chitosan hydrogel [81]. The experiments were performed to evaluate the microgel's ability to reach 42–46 °C that is required for cell apoptosis and increased drug release for the microgel's shrinking. Parameters were also monitored to estimate the specific absorption rate (SAR).

The immobilization of the SPION@CA in the microgel influenced the SAR values in comparison to non-microgel media, while the microgel modified with SPION suspension successfully generated heat despite its high viscosity under the application of the alternating magnetic field. As shown in Fig. 8 the temperature rise depends on the experimental conditions applied to the suspension while taking the measurements. Measurements presented in Fig. 8a were performed at 386 kHz, showing that the rise in the amplitude causes an increase in temperature. The target temperature was up to 46 °C, which could not be reached while applying such conditions. Even the amplitude of about 30 kA m⁻¹ was insufficient, and the temperature was starting to stabilize at about 40 °C. The following measurement was performed for a frequency of AMF of about 488 kHz. As can be seen, the temperature rise was much higher than for lower frequency. For a field of about 25 kA m⁻¹, the suspension reached 40 °C, and with a field intensity of about 30 kA m⁻¹, the temperature rose to 45 °C see Fig. 8b. Next, the frequency was subsequently increased to 633 kHz. When the amplitude is too low, e.g., 5 kA m⁻¹, the microgel solution does not heat sufficiently to reach the therapeutic temperature. As expected, a lower field is needed to reach the target temperature (as compared to 488 kHz frequency), with 20 kA m⁻¹ being sufficient. Figure 8c shows the curves recorded under these conditions. Another rise in the frequency of the AMF would be too large. For human safety from high-frequency field exposure, the maximum value of the product of field amplitude and frequency is set by the Brezovich limit of about

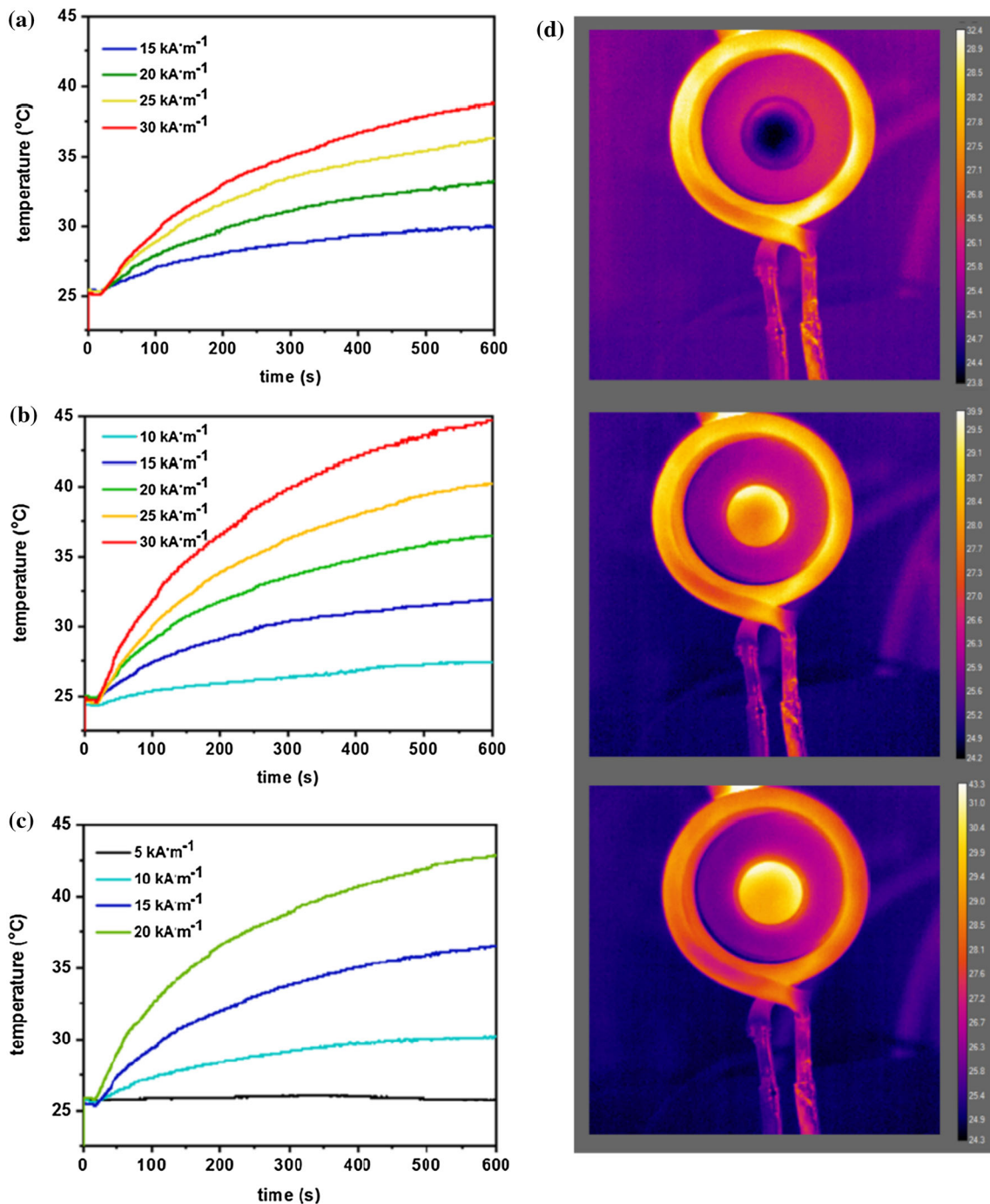


Figure 8 Heating of the gel based on SPION@CA at various frequencies and amplitudes of the magnetic field (a) 386 kHz, (b) 488 kHz, (c) 633 kHz, and (d) thermal images of gel under the 20 kA m⁻¹ after 10 s, 300 s, and 600 s of treatment.

$f \cdot H = 4.85 \times 10^{-8} \text{ A m}^{-1} \text{ s}^{-1}$ [82] Fig. 8d shows the thermal images of the *p*(NIPA-BISS-SPION@CA) microgel solution heating under the alternating magnetic field (the internal sphere on the image is a microgel placed on the Petri dish, while the ring is a coil). As can be seen, initially, the solution had room

temperature, while its temperature raised after the magnetic field treatment.

Note that the microgel solution was stable after the MH measurements, so the SPION@CA did not agglomerate after the application of the AMF. Additionally, the specific absorption rates (SAR) were

estimated for the conditions in which the target temperature was reached in 10 min. similarly to the procedure described in the literature [83]. The SAR values for the conditions where the temperature increased above 42 °C are presented in Table. 2.

MH results reveal the potential of the proposed microgel for magnetic hyperthermia applications. The following section presents its possible use as a potent carrier for doxorubicin delivery and stimuli-responsive release of the drug.

Drug loading and release

Next, the usefulness of microgel as doxorubicin (anti-cancer drug) carrier was investigated. The drug loading capacity (DLC) was evaluated using Eq. (1):

$$\text{DLC}\% = \frac{m_{\text{total}}^{\text{DOX}} - m_{\text{free}}^{\text{DOX}}}{m_{\text{microgel}}} \times 100\%, \quad (1)$$

where $m_{\text{total}}^{\text{DOX}}$ is the total mass of DOX used in the loading process, $m_{\text{free}}^{\text{DOX}}$ is the mass of DOX that was not bound to the microgel, and m_{microgel} is the mass of the dry microgel. The determined DLC equaled ca. 16%. The loading efficiency (LE), evaluated using Eq. (2), was ca. 89%:

$$\text{LE}\% = \frac{m_{\text{total}}^{\text{DOX}} - m_{\text{free}}^{\text{DOX}}}{m_{\text{total}}^{\text{DOX}}} \times 100\%, \quad (2)$$

The influence of pH and GSH on the release efficiency of DOX from the microgel at two selected temperatures, 37 °C and 42 °C (the temperature was maintained in the water bath), was evaluated. As Fig. 9 shows, the release behavior depended on the pH, temperature, and presence of the reducing agent. It was found that in the absence of GSH at pH 5 and 7, and at both selected temperatures only burst releases were observed, i.e., a significant increase in DOX release during the initial 1.5 h is readily visible, then after 3 h, plateaus were formed. In the presence of GSH, both fast and slow/long-term releases were observed. After a burst release, further increases in the concentration of released DOX are seen. It seems that the degradation of the polymer network of the

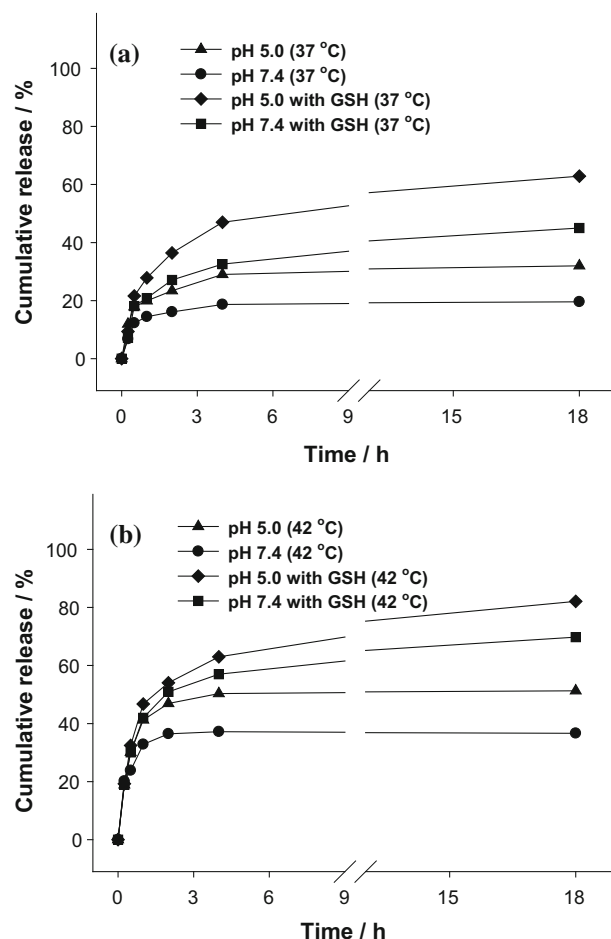


Figure 9 DOX release profiles from DOX-loaded microgels for different temperatures, pH values, and the presence of GSH at 37 °C (a) and 42 °C (b).

microgels also influences the release of drug [14, 84]. The smallest amount of DOX was released from the microgel at pH 7.4, 37 °C, and in the absence of GSH. The electrostatic attraction between DOX and the microgel caused only ca. 20% of DOX to be released after several hours in such conditions. The higher cumulative release was observed at pH 5.0. Cumulative release at pH 5.0, 37 °C, and without GSH increased to ca. 38% after 18 h. At this pH, the electrostatic interactions between DOX and the microgel were weaker because part of the carboxylic groups in the microgel were protonated. The addition of GSH in all cases led to the increased cumulative release, i.e., in pH 5 after 18 h, it reached ca. 63% of DOX.

The additional increase in cumulative release, due to the addition of GSH, can be explained by the synergic effects: competition between DOX and GSH

Table 2 SAR values for certain MH parameters

AC field (kA m ⁻¹)	Frequency (kHz)	SAR (W g ⁻¹)
25	488	104.4 ± 12.3
30	488	157.5 ± 17.1
20	633	141.6 ± 18.2

(GSH also contains protonated amine group) in the interactions with the ionized carboxylic groups and loosening of the structure of the microgel by degradation of the polymer network. It can be also noted that under hyperthermia conditions (42 °C) cumulative release of DOX increased in all investigated cases. For example, an increase in temperature from 37 to 42 °C led to an increase of DOX release from 63 to 82%, respectively. It should be pointed out here that under conditions characteristic to the blood circulatory system (pH 7.4, T=37 °C, and absence of GSH) the cumulative release measured after 18 h was 20%, while this value increased significantly, to 82%, under hyperthermia and the conditions existing in certain cancer cells (pH 5.0, $C_{\text{GSH}} \sim 40$ mM).

Next, to determine which drug release model best describes the kinetics of DOX release from the *p*(NIPA-BISS-SPION@CA) microgel, the data were fitted to the five commonly used models (Table 1). The release kinetics were evaluated via the correlation coefficient (R^2) of linearized equations presented in Table 1, and the results are shown in Table 3. R^2 is a numerical value from 0 to 1 and the closest fit is denoted by the R^2 value closest to 1. The R^2 values for the Korsmeyer–Peppas and Gompertz models were found to have the highest values (Table 3). It seems, therefore, that models which describe drug release from a polymeric system (Korsmeyer–Peppas), and the release profiles of drugs having good solubility and intermediate release rate (Gompertz), are suitable for describing the DOX release from *p*(NIPA-BISS-SPION@CA) microgels.

Cytotoxicity investigations

Next, in the in vitro studies, MCF-10A non-tumorigenic human breast epithelial and MCF-7 breast cancer cell lines were loaded with a hydrogel containing DOX. As Fig. 10 shows, this research confirmed that the microgel was nontoxic against all cells in the entire range of tested concentrations. However, at higher concentrations, cell viability decreased but such values of cell growth indicate good survivability when exposed to the unloaded/drug-free microgel. Moreover, free DOX and *p*(NIPA-BISS-SPION@CA) microgel loaded with DOX exhibited similar cytotoxicity; for the MCF-7 cells, the IC₅₀ value equaled 0.162 and 0.128 μM for free DOX and DOX-loaded microgel, respectively. Interesting results were achieved for the MCF-10A cell line (healthy cells) see Fig. 11. In the case of treatment of healthy cells with the free DOX, the IC₅₀ value was equal to 0.21 μM . When DOX loaded microgel was used, the determination of IC₅₀ value was not possible in the range of tested concentrations. This phenomenon can be explained through the smaller release of drug from microgel carrier under the conditions of healthy cells.

In addition to typical cytotoxicity studies, the impact of the carriers on the selected cells was also investigated using a confocal microscope. All the cells were treated with a 0.01 μM concentration of drug-loaded microgel. The nuclei of the cells that were previously treated with the Hoechst dye, which stains cell nuclei, emitted blue-cyan light, while DOX emitted red light. Figure 11 shows 3D images of healthy (MCF-10A) and cancer cells (MCF-7) after

Table 3 The release kinetics of DOX

Kinetic Model	<i>p</i> (NIPA-BISS-SPION@CA)/DOX 37 °C		<i>p</i> (NIPA-BISS-SPION@CA)/DOX/GSH 37 °C		<i>p</i> (NIPA-BISS-SPION@CA)/DOX 42 °C		<i>p</i> (NIPA-BISS-SPION@CA)/DOX/GSH 42 °C	
	pH 5	pH 7	pH 5	pH 7	pH 5	pH 7	pH 5	pH 7
	First-order	0.7809	0.5246	0.6915	0.7649	0.3600	0.2429	0.6482
Korsmeyer–Peppas	0.9348	0.8887	0.9729	0.989	0.8932	0.9080	0.9407	0.9108
Higuchi	0.823	0.7302	0.9272	0.9582	0.5203	0.4348	0.8991	0.8369
Gompertz	0.9753	0.9417	0.9907	0.9643	0.9505	0.9233	0.9827	0.9855
Weibull	0.4087	0.2654	0.5462	0.5603	0.1916	0.1317	0.5117	0.4394

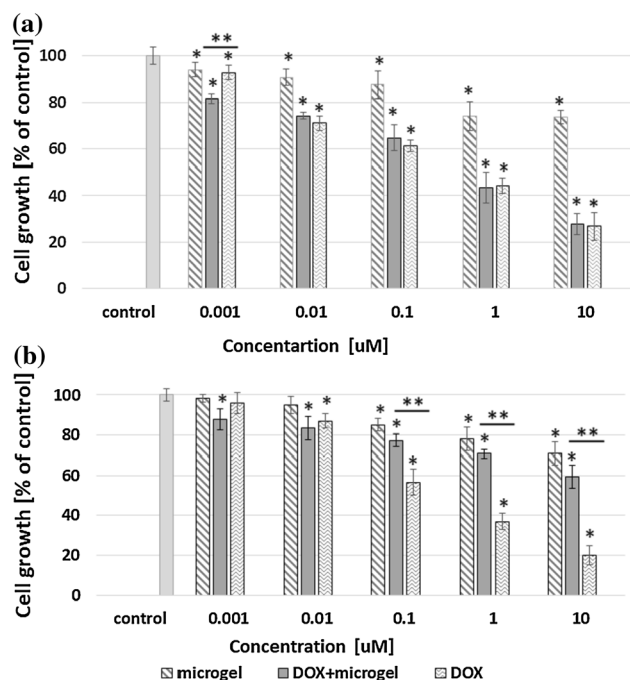


Figure 10 Results of MTT assay using MCF-7 (a) and MCF-10A (b) cell lines after 72-h treatment with free DOX, drug-loaded and drug-free *p*(NIPA-BISS-SPION@CA) microgels. One-way ANOVA was used to test for statistical significance. Differences from the control sample were marked with *, whereas ** marked differences between groups. The difference was considered significant for $P < 0.05$.

72 h interactions with *p*(NIPA-BISS-SPION@CA) microgels loaded with DOX. As is visible, in cancer cells DOX (red color) is present mainly in nuclei. In healthy cells DOX is also present in nuclei; however, the red color is not as intensive as in the nuclei of cancer cells, moreover, red color is well visible in the cytoplasm (see side panels). The significantly larger accumulation of DOX in nuclei of MCF-7 can explain the much greater toxicity of the DOX-loaded microgel against cancer cells than the healthy cells. The obtained results suggest that the microgels can improve the effectiveness of cancer treatment with DOX by protecting healthy cells.

Base on the stability investigations, it can be assumed that *p*(NIPA-BISS-SPION@CA) microgels are stable in the intercellular space. The most likely mechanism of transport of the *p*(NIPA-BISS-SPION@CA) microgel into the cell is the process of endocytosis [85]. In the reducing environment of the cell, the polymer network degrades and SPION@CAs can accumulate in lysosomes, where they are

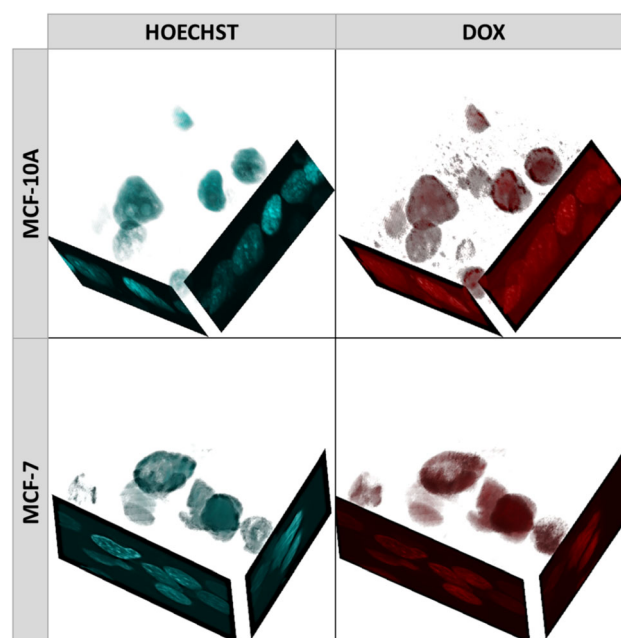


Figure 11 Confocal 3D images of MCF-10A and MCF-7 cell lines after 72 h incubation with DOX-loaded *p*(NIPA-BISS-SPION@CA) microgels. Cell nuclei were stained with Hoechst dye (cyan color); the red color indicates DOX.

gradually degraded, with co-localization with dextranses and iron buildup [86, 87]. When microgels are loaded with DOX, the release of the drug leads to cell death.

Conclusions

The applied precipitation polymerization via the semi-batch method proved useful in the synthesis of *p*(NIPA-BISS-SPION@CA) microgel containing superparamagnetic nanoparticles (SPION@CA). Controlled feeding of SPION@CA to the reactor allowed for their successful incorporation, confirmed using scanning electron microscopy coupled with EDS/EDX detector. The performed experiments indicated that the microgel solution was stable across a wide range of temperatures and ionic strengths, as well as in the blood plasma at 37 °C. Using derivatives of cystine as cross-linkers makes the microgels degradable in the presence of glutathione. The –S–S– bonds in the polymer network were reduced by GSH and cleaved. It was found that by applying magnetic hyperthermia, the temperature of microgel solution can be increased using the alternating magnetic field up to 42 °C. The presence of the carboxylic group in

the cross-linker allowed a load of doxorubicin into the microgels and then the efficient release of the drug under characteristic pH (5.0, 7.4) and temperature (37 °C, 42 °C, where the temperature was maintained in the water bath). The effect of the presence or absence of GSH was also evaluated. It was found that a shift in environmental conditions from those corresponding to the blood circulatory system, to those characteristic of the affected/cancer cells, triggered a release of a significant amount of loaded doxorubicin. Moreover, applying hyperthermia led to the enhanced release of anticancer drug. In vitro experiments proved that the DOX-loaded microgel compared to the free drug was similarly cytotoxic for cancer cells (MCF-7) but much less toxic for healthy cells (MCF-10A). This makes the obtained new microgel an interesting candidate for a drug carrier whose efficiency can be enhanced using a magnetic field. By applying an appropriate alternating magnetic field, due to the presence of immobilized superparamagnetic nanoparticles in the polymer network, it is possible to locally increase the temperature to or above 42 °C. This increase in temperature can improve the efficient release of the drug and can induce apoptosis of cancer cells. In line with these features, microgels *p*(NIPA-BISS-SPION@CA) are promising for combinatorial cancer therapy involving hyperthermia and chemotherapy.

Acknowledgements

This work was supported by the National Center for Research and Development (Poland) under grant number TANGO-V-A/0051/2021-00.

Declarations

Conflict of interest The authors declare no conflict of interest.

Open Access

This article is licensed under a Creative Commons Attribution 4.0 International License, which permits use, sharing, adaptation, distribution and reproduction in any medium or format, as long as you give appropriate credit to the original author(s) and the source, provide a link to the Creative Commons licence, and indicate if changes were made. The

images or other third party material in this article are included in the article's Creative Commons licence, unless indicated otherwise in a credit line to the material. If material is not included in the article's Creative Commons licence and your intended use is not permitted by statutory regulation or exceeds the permitted use, you will need to obtain permission directly from the copyright holder. To view a copy of this licence, visit <http://creativecommons.org/licenses/by/4.0/>.

References

- [1] Xu ZW, Lu X, Zhu YH, Xiong CY, Li B, Li SL, Zhang Q, Tian XH, Li DD, Tian YP (2022) Prolongation excitation wavelength of two-photon active photosensitizer for near-infrared light-induced in vitro photodynamic therapy. *J Mol Struct* 1254:132030
- [2] Chang MQ, Feng W, Ding L, Zhang HG, Dong CH, Chen Y, Shi JL (2022) Persistent luminescence phosphor as in-vivo light source for tumoral cyanobacterial photosynthetic oxygenation and photodynamic therapy. *Bioact Mater* 10:131–144
- [3] Su CH, Ren XJ, Yang F, Li B, Wu H, Li H, Nie F (2022) Ultrasound-sensitive siRNA-loaded nanobubbles fabrication and antagonism in drug resistance for NSCLC. *Drug Deliv* 29:99–110
- [4] Yang ZL, Lin Z, Yang J, Wang J, Yue J, Liu B, Jiang LL (2022) Fabrication of porous noble metal nanoparticles based on laser ablation toward water and dealloying for biosensing. *Appl Surf Sci* 579:152130
- [5] Kono M, Komatsuda H, Yamaki H, Kumai T, Hayashi R, Wakisaka R, Nagato T, Ohkuri T, Kosaka A, Ohara K, Kishibe K, Takahara M, Katada A, Hayashi T, Kobayashi H, Harabuchi Y (2022) Immunomodulation via FGFR inhibition augments FGFR1 targeting T-cell based antitumor immunotherapy for head and neck squamous cell carcinoma. *Oncoimmunology* 11(1):2021619
- [6] Levin BA, Lama DJ, Sussman J, Guan TY, Rao M, Tobler J, Verma S, Sidana A (2022) Does the type of biopsy used for diagnosis impact subsequent treatment selection in prostate cancer patients? *Aging Male* 25:23–28
- [7] Ta HT, Dass CR, Dunstan DE (2008) Injectable chitosan hydrogels for localised cancer therapy. *J Control Release* 126:205–216
- [8] Wilson RJ, Li Y, Yang GZ, Zhao CX (2022) Nanoemulsions for drug delivery. *Particuology* 64:85–97
- [9] Rao Y, Li RW, Liu SX, Meng LC, Wu QL, Yuan QP, Liang H, Qin M (2022) Enhanced bioavailability and biosafety of

- cannabidiol nanomicelles for effective anti-inflammatory therapy. *Particuology* 69:1–9
- [10] Lotter C, Alter CL, Bolten JS, Detampel P, Palivan CG, Einfalt T, Huwyler J (2022) Incorporation of phosphatidylserine improves efficiency of lipid based gene delivery systems. *Eur J Pharm Biopharm* 172:134–143
- [11] Shu SR, Liu XP, Xu M, Lin YD, Li RM (2022) The inhibitory role of si-UBB delivered by degradable dendrimers-based lipid nanoparticles in ovarian cancer. *Cancer Nanotechnol.*
- [12] Huang SJ, Huang X, Yan HS (2022) Peptide dendrimers as potentiators of conventional chemotherapy in the treatment of pancreatic cancer in a mouse model. *Eur J Pharm Biopharm* 170:121–132
- [13] Deng WT, Yan Y, Zhuang PP, Liu XX, Tian K, Huang WF, Li C (2022) Synthesis of nanocapsules blended polymeric hydrogel loaded with bupivacaine drug delivery system for local anesthetics and pain management. *Drug Deliv* 29:399–412
- [14] Mackiewicz M, Dagdelen S, Marcisz K, Waleka-Bargiel E, Stojek Z, Karbarz M (2021) Redox-degradable microgel based on poly(acrylic acid) as drug-carrier with very high drug-loading capacity and decreased toxicity against healthy cells. *Polym Degrad Stabil* 190:109652
- [15] Mackiewicz M, Romanski J, Drozd E, Gruber-Bzura B, Fiedor P, Stojek Z, Karbarz M (2017) Nanohydrogel with *N,N'*-bis(acryloyl)cystine crosslinker loading for high drug. *Int J Pharmaceut* 523:336–342
- [16] Mackiewicz M, Kaniewska K, Romanski J, Augustin E, Stojek Z, Karbarz M (2015) Stable and degradable microgels linked with cystine for storing and environmentally triggered release of drugs. *J Mater Chem B* 3:7262–7270
- [17] Queiroz PM, Barrioni BR, Nuncira J, Pereira MD (2022) Injectability study and rheological evaluation of Pluronic-derived thermosensitive hydrogels containing mesoporous bioactive glass nanoparticles for bone regeneration. *J Mater Sci* 57:13027–13042
- [18] Daneluti ALM, Guerra LO, Velasco MVR, Matos JD, Baby AR, Kalia YN (2021) Preclinical and clinical studies to evaluate cutaneous biodistribution, safety and efficacy of UV filters encapsulated in mesoporous silica SBA-15. *Eur J Pharm Biopharm* 169:113–124
- [19] Solomon S, Iqbal J, Albadarin AB (2021) Insights into the ameliorating ability of mesoporous silica in modulating drug release in ternary amorphous solid dispersion prepared by hot melt extrusion. *Eur J Pharm Biopharm* 165:244–258
- [20] Li HZ, Xu W, Li F, Zeng R, Zhang XM, Wang XW, Zhao SJ, Weng J, Li Z, Sun LP (2022) Amplification of anticancer efficacy by co-delivery of doxorubicin and lonidamine with extracellular vesicles. *Drug Deliv* 29:192–202
- [21] Kubiak A, Mackiewicz M, Karbarz M, Biesaga M (2022) Application of microgel as a sorbent for bisphenol analysis in liquid food samples. *Appl Sci-Basel* 12:441
- [22] Mackiewicz M, Romanski J, Drabczyk K, Waleka E, Stojek Z, Karbarz M (2019) Degradable, thermo-, pH- and redox-sensitive hydrogel microcapsules for burst and sustained release of drugs. *Int J Pharmaceut* 569:118589
- [23] Mackiewicz M, Romanski J, Krug P, Mazur M, Stojek Z, Karbarz M (2019) Tunable environmental sensitivity and degradability of nanogels based on derivatives of cystine and poly(ethylene glycols) of various length for biocompatible drug carrier. *Eur Polym J* 118:606–613
- [24] Liu LY, Zhang DD, Song XX, Guo M, Wang ZW, Geng F, Zhou XT, Nie SP (2022) Compound hydrogels derived from gelatin and gellan gum regulates the release of anthocyanins in simulated digestion. *Food Hydrocolloid* 127:107487
- [25] Anooj ES, Charumathy M, Sharma V, Vibala BV, Gopukumar ST, Jainab SIB, Vallinayagam S, Nanogels, (2021) An overview of properties, biomedical applications, future research trends and developments. *J Mol Struct* 1239:130446
- [26] Plamper FA, Richtering W (2017) Functional microgels and microgel systems. *Acc Chem Res* 50:131–140
- [27] Dai ZJ, Ngai T (2013) Microgel particles: the structure-property relationships and their biomedical applications. *J Polym Sci Pol Chem* 51:2995–3003
- [28] Karbarz M, Mackiewicz M, Kaniewska K, Marcisz K, Stojek Z (2017) Recent developments in design and functionalization of micro- and nanostructural environmentally-sensitive hydrogels based on *N*-isopropylacrylamide. *Appl Mater Today* 9:516–532
- [29] Kubiak A, Mackiewicz M, Biesaga M, Karbarz M (2021) Highly efficient removal of bisphenols from aqueous solution using environmental-sensitive microgel. *J Environ Chem Eng.* 9(1):10497
- [30] Mackiewicz M, Stojek Z, Karbarz M (2017) Unusual swelling behavior of core-shell microgels built from polymers exhibiting lower critical solubility temperature. *Eur Polym J* 95:314–322
- [31] Mackiewicz M, Romanski J, Karbarz M (2014) New ampholytic microgels based on *N*-isopropylacrylamide and alpha-amino acid: changes in swelling behavior as a function of temperature, pH and divalent cation concentration. *Rsc Adv* 4:48905–48911
- [32] Xia XJ, Mugo SM, Zhang Q (2022) Responsive microgels-based wearable devices for sensing multiple health signals. *Chem Eng J* 427:130903
- [33] Farmanbordar H, Amini-Fazl MS, Mohammadi R (2021) pH-Sensitive silica-based core-shell nanogel prepared via RAFT polymerization: investigation of the core size effect

- on the release profile of doxorubicin. *New J Chem* 45:21824–21833
- [34] Islam MR, Lyon LA (2020) Deswelling studies of pH and temperature-sensitive ultra-low cross-linked microgels with cross-linked cores. *Colloid Polym Sci* 298:395–405
- [35] Ling X, Tu JS, Wang JQ, Shajii A, Kong N, Feng C, Zhang Y, Yu MK, Xie T, Bharwani Z, Aljaeid BM, Shi BY, Tao W, Farokhzad OC (2019) Glutathione-responsive prodrug nanoparticles for effective drug delivery and cancer therapy. *ACS Nano* 13:357–370
- [36] Sanson N, Rieger J (2010) Synthesis of nanogels/microgels by conventional and controlled radical crosslinking copolymerization. *Polym Chem-Uk* 1:965–977
- [37] Nayak S, Lyon LA (2005) Soft nanotechnology with soft nanoparticles. *Angew Chem* 44:7686–7708
- [38] Karg M, Pich A, Hellweg T, Hoare T, Lyon LA, Crassous JJ, Suzuki D, Gumerov RA, Schneider S, Potemkin II, Richtering W (2019) Nanogels and microgels: from model colloids to applications, recent developments, and future trends. *Langmuir* 35:6231–6255
- [39] Wei LX, Yang HF, Hong JD, He ZH, Deng CL (2019) Synthesis and structure properties of Se and Sr co-doped hydroxyapatite and their biocompatibility. *J Mater Sci* 54:2514–2525
- [40] Cao-Luu NH, Pham QT, Yao ZH, Wang FM, Chern CS (2019) Synthesis and characterization of PNIPAM microgel core-silica shell particles. *J Mater Sci* 54:7503–7516
- [41] Merland T, Waldmann L, Guignard O, Tetry MC, Wirotius AL, Lapeyre V, Garrigue P, Nicolai T, Benyahia L, Ravaine V (2022) Thermo-induced inversion of water-in-water emulsion stability by bis-hydrophilic microgels. *J Colloid Interf Sci* 608:1191–1201
- [42] Muratov AD, Markina AA, Pergushov DV, Avetisov VA (2021) Modeling of thermosensitive stereoregular polymers within the coarse-grained force field: Poly(*N*-isopropylacrylamide) as a benchmark case. *Phys Fluids* 33(8):087110
- [43] Zhan Y, Goncalves M, Yi PP, Capelo D, Zhang YH, Rodrigues J, Liu CS, Tomas H, Li YL, He PX (2015) Thermo/redox/pH-triple sensitive poly(*N*-isopropylacrylamide-co-acrylic acid) nanogels for anticancer drug delivery. *J Mater Chem B* 3:4221–4230
- [44] Cheng C, Xia DD, Zhang XL, Chen L, Zhang QQ (2015) Biocompatible poly(*N*-isopropylacrylamide)-*g*-carboxymethyl chitosan hydrogels as carriers for sustained release of cisplatin. *J Mater Sci* 50:4914–4925
- [45] Zhang YM, Liu YH, Liu Y (2020) Cyclodextrin-based multistimuli-responsive supramolecular assemblies and their biological functions. *Adv Mater* 32(3):1806158
- [46] He L, Sun M, Cheng X, Xu Y, Lv XD, Wang X, Tang RP (2019) pH/redox dual-sensitive platinum (IV)-based micelles with greatly enhanced antitumor effect for combination chemotherapy. *J Colloid Interf Sci* 541:30–41
- [47] Es Sayed J, Meyer C, Sanson N, Perrin P (2020) Oxidation-responsive emulsions stabilized by cleavable metallo-supramolecular cross-linked microgels. *ACS Macro Lett* 9:1040–1045
- [48] Li XT, Yuan SC, Shea KJ, Qiu G, Lu XH, Zhang RY (2018) Redox/temperature responsive nonionic nanogel and photonic crystal hydrogel: comparison between *N*, *N'*-Bis(acryloyl)cystamine and *N*, *N'*-methylenebisacrylamide. *Polymer* 137:112–121
- [49] Zhang HY, Sun CY, Adu-Frimpong M, Yu JN, Xu XM (2019) Glutathione-sensitive PEGylated curcumin prodrug nanomicelles: preparation, characterization, cellular uptake and bioavailability evaluation. *Int J Pharmaceut* 555:270–279
- [50] Peng H, Huang XB, Melle A, Karperien M, Pich A (2019) Redox-responsive degradable prodrug nanogels for intracellular drug delivery by crosslinking of amine-functionalized poly(*N*-vinylpyrrolidone) copolymers. *J Colloid Interf Sci* 540:612–622
- [51] Jeong GW, Jeong YI, Nah JW (2019) Triggered doxorubicin release using redox-sensitive hyaluronic acid-*g*-stearic acid micelles for targeted cancer therapy. *Carbohyd Polym* 209:161–171
- [52] Kailasa SK, Joshi DJ, Kateshiya MR, Koduru JR, Malek NI (2022) Review on the biomedical and sensing applications of nanomaterial-incorporated hydrogels. *Mater Today Chem* 23:100746
- [53] Mackiewicz M, Marcisz K, Strawski M, Romanski J, Stojek Z, Karbarz M (2018) Modification of gold electrode with a monolayer of self-assembled microgels. *Electrochim Acta* 268:531–538
- [54] Mackiewicz M, Karbarz M, Romanski J, Stojek Z (2016) An environmentally sensitive three-component hybrid microgel. *Rsc Adv* 6:83493–83500
- [55] Mackiewicz M, Rapecki T, Stojek Z, Karbarz M (2014) Environmentally sensitive, quickly responding microgels with lattice channels filled with polyaniline. *J Mater Chem B* 2:1483–1489
- [56] Jia XB, Li XJ, Lv CN, Wang SY, Dong WP (2020) Intelligent magnetic imprinted nanoparticles for efficient lysozyme separation from egg whites and sustained antibacterial activity. *J Mater Sci* 55:11572–11581
- [57] Wen X, Qiao XL, Han X, Niu LB, Huo L, Bai GY (2016) Multifunctional magnetic branched polyethylenimine nanogels with in-situ generated Fe₃O₄ and their applications as dye adsorbent and catalyst support. *J Mater Sci* 51:3170–3181

- [58] Nadeem M, Khan R, Shah NS, Bangash IR, Abbasi BH, Hano C, Liu CZ, Ullah S, Hashmi SS, Nadhman A, Celli J (2022) A review of microbial mediated iron nanoparticles (IONPS) and its biomedical applications. *Nanomaterials-Basel* 12(1):130
- [59] Eivazzadeh-Keihan R, Radinekiyan F, Maleki A, Bani MS, Azizi M (2020) A new generation of star polymer: magnetic aromatic polyamides with unique microscopic flower morphology and in vitro hyperthermia of cancer therapy. *J Mater Sci* 55:319–336
- [60] Eivazzadeh-Keihan R, Radinekiyan F, Asgharnasl S, Maleki A, Bahreinizad H (2020) A natural and eco-friendly magnetic nanobiocomposite based on activated chitosan for heavy metals adsorption and the in-vitro hyperthermia of cancer therapy. *J Mater Res Technol* 9:12244–12259
- [61] Thanh DTM, Phuong NT, Hai DT, Giang HN, Thom NT, Nam PT, Dung NT, Giersig M, Osial M (2022) Influence of experimental conditions during synthesis on the physicochemical properties of the SPION/hydroxyapatite nanocomposite for magnetic hyperthermia application. *Magnetochemistry* 8(8):90
- [62] Eid MM, Ismail AM, Elshahid ZA, Abd Elzaher FH, Mahmoud K, El-Manawaty M (2022) Plasmonic Superparamagnetic SPION@Ag@chitosan Core-shell: uptake and nitric oxide inhibition by colorectal cell lines. *J Inorg Organomet P* 32:931–940
- [63] Eivazzadeh-Keihan R, Asgharnasl S, Bani MS, Radinekiyan F, Maleki A, Mahdavi M, Babaniamansour P, Bahreinizad H, Shalan AE, Lanceros-Mendez S (2021) Magnetic copper ferrite nanoparticles functionalized by aromatic polyamide chains for hyperthermia applications. *Langmuir* 37:8847–8854
- [64] Palzer J, Eckstein L, Slabu I, Reisen O, Neumann UP, Roeth AA (2021) Iron oxide nanoparticle-based hyperthermia as a treatment option in various gastrointestinal malignancies. *Nanomaterials-Basel* 11:3013
- [65] Musielak M, Piotrowski I, Suchorska WM (2019) Superparamagnetic iron oxide nanoparticles (SPIONs) as a multifunctional tool in various cancer therapies. *Rep Pract Oncol Radi* 24:307–314
- [66] Li ZG, Li YZ, Chen C, Cheng Y (2021) Magnetic-responsive hydrogels: from strategic design to biomedical applications. *J Control Release* 335:541–556
- [67] Gaweda W, Osial M, Zuk M, Pekala M, Bilewicz A, Krysinski P (2020) Lanthanide-doped SPIONs bioconjugation with trastuzumab for potential multimodal anticancer activity and magnetic hyperthermia. *Nanomaterials-Basel* 10(2):288
- [68] Cascone S (2017) Modeling and comparison of release profiles: effect of the dissolution method. *Eur J Pharm Sci* 106:352–361
- [69] Lennernas H (2007) Modeling gastrointestinal drug absorption requires more in vivo biopharmaceutical data: experience from in vivo dissolution and permeability studies in humans. *Curr Drug Metab* 8:645–657
- [70] Costa P, Sousa Lobo JM (2001) Modeling and comparison of dissolution profiles. *Eur J Pharm Sci* 13:123–133
- [71] Kamaly N, Yameen B, Wu J, Farokhzad OC (2016) Degradable controlled-release polymers and polymeric nanoparticles: mechanisms of controlling drug release. *Chem Rev* 116:2602–2663
- [72] Zhang S, Fan XX, Zhang GJ, Wang WD, Yan L (2021) Preparation, characterization, and in vitro release kinetics of doxorubicin-loaded magnetosomes. *J Biomater Appl* 36(8):1469–1483
- [73] Das SK, Ghosh GK (2022) Hydrogel-biochar composite for agricultural applications and controlled release fertilizer: a step towards pollution free environment. *Energy* 242:122977
- [74] Huang CQ, Liao HY, Liu XH, Xiao M, Liao SY, Gong S, Yang FJ, Shu XG, Zhou XH (2022) Preparation and characterization of vanillin-chitosan Schiff base zinc complex for a novel Zn²⁺ sustained released system. *Int J Biol Macromol* 194:611–618
- [75] Tang L, Wang L, Yang X, Fen YY, Li Y, Feng W (2021) Poly(N-isopropylacrylamide)-based smart hydrogels: Design, properties and applications. *Prog Mater Sci* 115:100702
- [76] Kobayashi H, Halver R, Sutmann G, Winkler RG (2017) Polymer conformations in ionic microgels in the presence of salt: theoretical and mesoscale simulation results. *Polymers (Basel)* 9:15
- [77] Gonzalez-Mozuelos P (2016) Effective electrostatic interactions among charged thermo-responsive microgels immersed in a simple electrolyte. *J Chem Phys* 144:054902
- [78] Cao ZQ, Zhou XT, Wang GJ (2016) Selective release of hydrophobic and hydrophilic cargos from multi-stimuli-responsive nanogels. *Acs Appl Mater Inter* 8:28888–28896
- [79] Gaulding JC, Smith MH, Hyatt JS, Fernandez-Nieves A, Lyon LA (2012) Reversible inter- and intra-microgel cross-linking using disulfides. *Macromolecules* 45:39–45
- [80] Dhamecha D, Movsas R, Sano U, Menon JU (2019) Applications of alginate microspheres in therapeutics delivery and cell culture: past, present and future. *Int J Pharmaceut* 569:118627
- [81] Eivazzadeh-Keihan R, Radinekiyan F, Maleki A, Bani MS, Hajizadeh Z, Asgharnasl S (2019) A novel biocompatible core-shell magnetic nanocomposite based on cross-linked

- chitosan hydrogels for in vitro hyperthermia of cancer therapy. *Int J Biol Macromol* 140:407–414
- [82] Lee JH, Kim B, Kim Y, Kim SK (2021) Ultra-high rate of temperature increment from superparamagnetic nanoparticles for highly efficient hyperthermia. *Sci Rep* 11:4969
- [83] Eivazzadeh-Keihan R, Maleki A (2021) Design and synthesis of a new magnetic aromatic organo-silane star polymer with unique nanoplate morphology and hyperthermia application. *J Nanostructure Chem* 11:751–767
- [84] Gray DM, Town AR, Niezabitowska E, Rannard SP, McDonald TO (2022) Dual-responsive degradable core-shell nanogels with tuneable aggregation behaviour. *Rsc Adv* 12:2196–2206
- [85] Kruger TM, Givens BE, Lansakara TI, Bell KJ, Mohapatra H, Salem AK, Tivanski AV, Stevens LL (2018) Mechanosensitive endocytosis of high-stiffness, submicron microgels in macrophage and hepatocarcinoma cell lines. *Acs Appl Bio Mater* 1:1254–1265
- [86] Banobre-Lopez M, Teijeiro A, Rivas J (2013) Magnetic nanoparticle-based hyperthermia for cancer treatment. *Rep Pract Oncol Radi* 18:397–400
- [87] Jiao Q, Li LW, Mu QX, Zhang Q (2014) Immunomodulation of Nanoparticles in Nanomedicine Applications. *Biomed Res Int* 2014:1–19

Publisher's Note Springer Nature remains neutral with regard to jurisdictional claims in published maps and institutional affiliations.